

Heterogeneous network estimation for single-cell transcriptomic data via a joint regularized deep neural network

Jingyuan Yang, Tao Li, Tianyi Wang, Mengyun Wu *

School of Statistics and Data Science, Shanghai University of Finance and Economics

and

Shuangge Ma

Department of Biostatistics, Yale School of Public Health

Abstract

Network estimation has been a critical component of single-cell transcriptomic data analysis, which can provide crucial insights into the complex interplay among genes, facilitating uncovering the biological basis of human life at single-cell resolution. Despite notable achievements, existing methodologies often falter in their practicality, primarily due to their narrow focus on simplistic linear relationships and inadequate handling of cellular heterogeneity. To bridge these gaps, we propose a joint regularized deep neural network method incorporating a Mahalanobis distance-based K-means clustering (JRDNN-KM) to estimate multiple networks for various cell subgroups simultaneously, accounting for both unknown cellular heterogeneity and zero-inflation and, more importantly, complex nonlinear relationships among genes. We innovatively introduce a selection layer for network construction and develop homogeneous and heterogeneous hidden layers to accommodate commonality and specificity across multiple networks. Through simulations and applications to real single-cell transcriptomic data for multiple tissues and species, we show that JRDNN-KM constructs networks with more accuracy and biological interpretability and, meanwhile, identifies more accurate cell subgroups compared to the state-of-the-art methods in the literature. Building on the network construction, we further find hub genes with important biological implications and modules with statistical enrichment of biological processes.

Keywords: Graphical model; High-dimensional data analysis; Heterogeneous analysis; Network reconstruction; Nonlinear modeling

*The corresponding author, wu.mengyun@mail.shufe.edu.cn

1 Introduction

Exploring biological networks has become essential for unraveling the complex molecular systems that sustain life. These networks, involving sophisticated interactions among genes, proteins, and other cellular components, are crucial for grasping how cells behave, regulate themselves, and how diseases arise (Costanzo et al. 2019, Zheng & Tang 2024). In recent years, the explosion of biological data generated through high-throughput omics technologies has propelled the importance of network estimation research to unprecedented heights. Among the existing techniques, the Gaussian Graphical Models (GGMs) are perhaps the most popular. In GGMs, a sparse precision matrix (the inverse of the correlation matrix) is estimated to infer the network (Zhang & Zou 2014, Halama et al. 2024), describing the conditional dependencies between cellular components given the rests. The estimation procedure can be simplified into a set of sparse node-wise linear regression problems with simpler optimization. This conditional construction strategy takes a more systematic perspective than the simple unconditional construction (where “the other components” are ignored, such as the Pearson correlation-based methods), potentially leading to more biologically implicated results.

While these methods have indeed achieved notable success with bulk genomics data, they can encounter limitations due to population averaging. They also overlook the inherent diversity within cell populations, potentially leading to inaccurate network inferences. In contrast, single-cell transcriptomic data provide a unique opportunity to dissect cellular heterogeneity, allowing for more precise network reconstruction and the exploration of context-specific regulatory interactions (Gawad et al. 2016). Analyzing single-cell transcriptomic data is more challenging due to the cellular heterogeneity, dropout events, and low signal-to-noise ratio. Based on GGM, several network estimation methods have been

proposed. Among them, most studies are tailored to accommodate the zero-inflated expression patterns resulting from dropout events, such as HurdleNormal (McDavid et al. 2019), PLNet (Xiao et al. 2022), scLGM (Oh et al. 2023), and PC-zinb (Nguyen et al. 2023), and a few others take a different perspective to address the mean-correlation relationship (Wang et al. 2022). These methods show progress but rely on the assumption that the cells are identically and independently distributed, which is usually not true in single-cell transcriptomic data, and thus are still not practically useful.

A few other studies conduct a further step and additionally take into account the cellular heterogeneity and construct multiple networks for different cell subgroups, where the interactions, coordination, and other relationships among genes may vary. Examples include the Bayesian latent Gaussian graph mixture model (BLGGM) (Wu & Luo 2022), which can handle the unknown cellular heterogeneity and zero inflation simultaneously. Aside from the heterogeneity of the networks, the potentially shared common structures within cell subgroups have received great attention, as cells belonging to distinct subgroups are frequently derived from the same tissue. Motivated by some studies originally developed for bulk genomics data, which are based on the fused and group Lasso penalties, a few joint network estimation methods have been proposed for effectively accommodating both the heterogeneity and homogeneity among cell subgroups, as well as the unique characteristics of single-cell transcriptomic data. Examples include the joint Gaussian copula graphical model (Wu et al. 2020), GGM incorporating a Bayesian zero-inflated Poisson (ZIP) model (Dong et al. 2023), and kernelized multiview signed graph learning (Karaaslanli et al. 2023).

Despite considerable successes, the aforementioned GGM-based methods only focus on linear dependencies, limiting their ability to capture complex nonlinear relationships among genes that are involved in almost all biological processes. To fill this gap, a few studies

take advantage of the nonparametric or distribution-free technique to detect the potential nonlinear relationships, such as the tree-based GENIE3 method (Huynh-Thu et al. 2010), the nonparametric test-based locCSN method (Wang et al. 2021), and the distribution-free-based CS-CORE method (Su et al. 2023). However, these methods mostly adopt the unconditional construction strategy and were originally developed for a single network analysis and depend on the prior known cell subgroup information, which may still lose effectiveness under the practical scenarios with usually complex conditional dependence and unknown cellular heterogeneity.

In response to these limitations, this work develops a novel joint regularized deep neural network incorporating a Mahalanobis distance-based K-means clustering (JRDNN-KM) for single-cell transcriptomic data, achieving network estimation and cell subgroup identification simultaneously. A workflow of JRDNN-KM is presented in Figure 1. Significantly advancing from the published studies, by exploiting the neural network’s capacity for flexible function approximation, JRDNN-KM can capture various nonlinear dependencies and interactions among genes in different cell subgroups while concurrently handling zero-inflation. By employing sparse and similarity regularization techniques, we ensure that the networks also share some common structures, enabling a more comprehensive joint exploration of different cell subgroups. The inferred networks are further incorporated into the Mahalanobis distance-based K-means clustering for detecting unknown cell subgroups, with the advantage of accommodating both the mean and covariance heterogeneous among cells. We demonstrate the performance of JRDNN-KM through extensive simulations and real single-cell transcriptomic datasets from humans and mice. JRDNN-KM detects biologically sensible cell subgroups, hub genes, and modules, significantly contributing to revealing the biological mechanisms driving cellular processes.

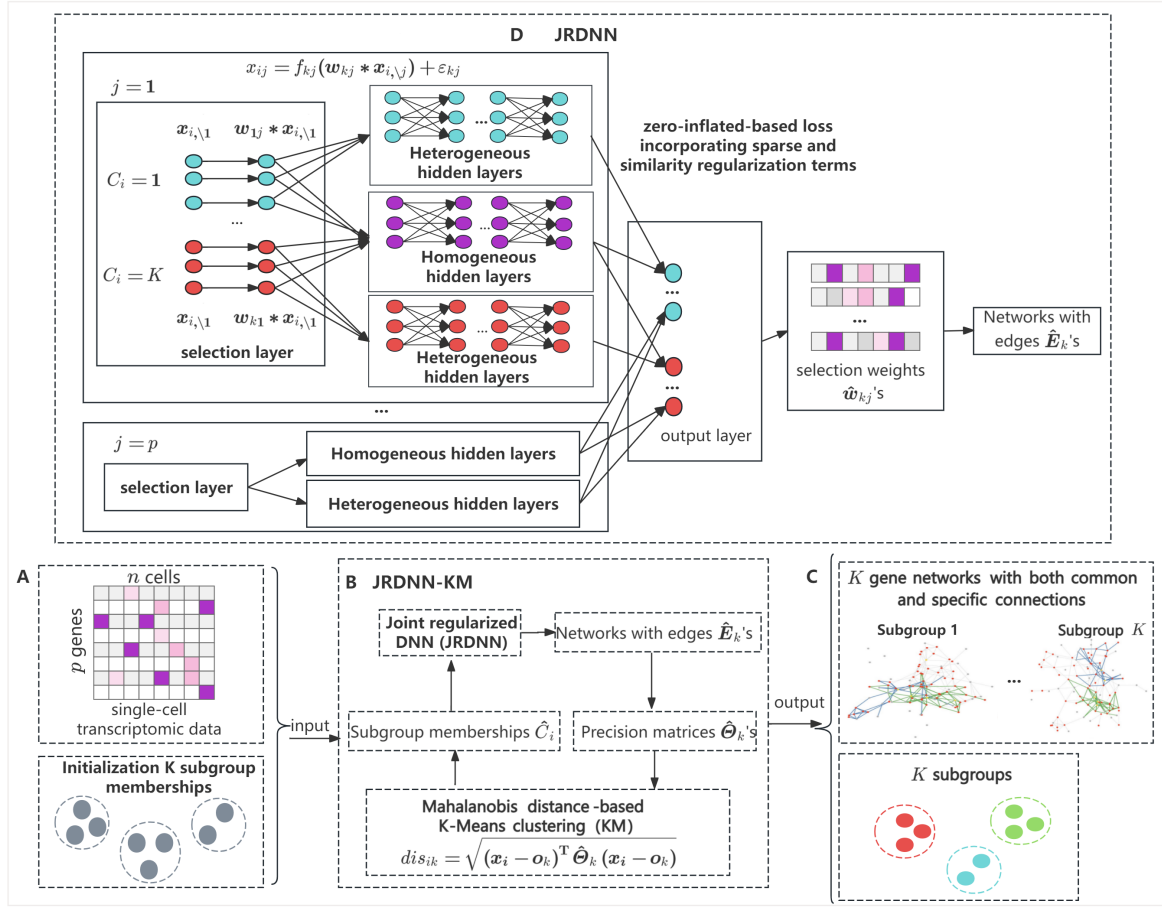


Figure 1: Workflow of JRDNN-KM. (A) Input: normalized single-cell transcriptome data \mathbf{x}_i 's and initialized cell subgroup memberships C_i 's. (B) JRDNN-KM: iterations between JRDNN and Mahalanobis distance-based K-means clustering. (C) Output: K networks for the K subgroups, with both common and specific edges, and estimated cell subgroup memberships. (D) Network structure of the proposed JRDNN, including the selection layers and combinations of homogeneous and heterogeneous hidden layers, with a zero-inflated-based loss incorporating sparse and similarity regularization terms.

2 Methods

Suppose there are n independent cells from K subgroups. For the i th cell, denote $C_i \in \{1, \dots, K\}$ as the subgroup assignment and $\mathbf{y}_i = (y_{i1}, \dots, y_{ip})^\top$ as the p -dimensional vector of the observed count transcriptomic data. In practice, \mathbf{y}_i has a high sparsity with zero-inflation due to the dropout event. Following the published studies (Booeshaghi & Pachter 2021, Hafemeister & Satija 2019), we conduct normalization using the R package *Seurat* and $\log(1 + x)$ transformation on \mathbf{y}_i 's to accommodate the library size and count nature and denote the processed continuous vector as $\mathbf{x}_i = (x_{i1}, \dots, x_{ip})^\top$.

2.1 Network estimation based on a joint regularized deep neural network

First, assume that the subgroup assignment is known, and for each subgroup, each gene is standardized to have a zero mean and unit variance. For accommodating the complex interplay among genes and zero inflation, when $C_i = k$, we consider a zero-inflated conditional Gaussian distribution as:

$$x_{ij} | \mathbf{x}_{i, \setminus j}; C_i = k \sim \mathcal{N}(f_{kj}(\mathbf{w}_{k, \setminus j} * \mathbf{x}_{i, \setminus j}), 1) \pi_j + \delta_0(x_{ij})(1 - \pi_j), \quad (1)$$

where $\mathbf{x}_{i, \setminus j} = (x_{i,1}, \dots, x_{i,j-1}, x_{i,j+1}, \dots, x_{i,p})^\top$, $\mathbf{w}_{k, \setminus j} = (w_{k,j1}, \dots, w_{k,j(j-1)}, w_{k,j(j+1)}, \dots, w_{k,jp})^\top$ is a sparse weight vector for $\mathbf{x}_{i, \setminus j}$, $*$ is the element-wise product, $f_{kj}(\mathbf{w}_{k, \setminus j} * \mathbf{x}_{i, \setminus j})$ is the mean parameter of Gaussian distribution with $f_{kj}(\cdot)$ being an arbitrarily nonparametric function, $\delta_0(\cdot)$ is a Dirac probability measure with a point mass at zero, and $0 \leq \pi_j \leq 1$ is the probability that the j th gene does not express zero caused by dropouts.

Based on Model (1), when $C_i = k$ and x_{ij} does not express zero, we have $x_{ij} = f_{kj}(\mathbf{w}_{k, \setminus j} * \mathbf{x}_{i, \setminus j}) + \varepsilon_{kj}$ with $\varepsilon_{kj} \sim \mathcal{N}(0, 1)$, where $f_{kj}(\cdot)$ describes the nonlinear relationships between

the j th gene and the others for the k th cell subgroup. Here, we introduce the sparse weight vector $\mathbf{w}_{k,j}$ to accommodate the sparse connections among genes and further construct the network. Specifically, if $w_{k,jl} \neq 0$ or $w_{k,lj} \neq 0$, the j th and l th genes have nonlinear conditional dependence and will be connected in the network. Model (1) can be treated as a nonlinear extension of the GGM-based node-wise regression (Cai et al. 2016, Wang et al. 2019).

For estimating $f_{kj}(\cdot)$ and the unknown parameters $\mathbf{w}_{k,j}$, we propose a joint regularized deep neural network (JRDNN) as shown in Figure 1(D). Specifically, for each j and k , the function represented by JRDNN can be written as (we omit the dependence on j to simplify notation):

$$g_k(\mathbf{z}_i; \mathbf{U}_k, \mathbf{w}_k) = T_k^{(M+1)} \begin{pmatrix} h \circ T_k^{(M)} \cdots h \circ T_k^{(2)} \circ h \circ T_k^{(1)}(\mathbf{w}_k * \mathbf{z}_i) \\ h \circ T_0^{(M)} \cdots h \circ T_0^{(2)} \circ h \circ T_0^{(1)}(\mathbf{w}_k * \mathbf{z}_i) \end{pmatrix}. \quad (2)$$

Here, $\mathbf{z}_i \in \mathbb{R}^{(p-1) \times 1}$ is an input vector, which is $\mathbf{x}_{i,j}$ in our network estimation procedure. We introduce a selection layer for \mathbf{w}_k and consider M hidden layers. Specifically, in (2), we consider two sub-fully connected neural networks, consisting of heterogeneous neurons and homogeneous neurons, respectively, where heterogeneous neurons and homogeneous neurons are connected with themselves but not connected with each other. Specifically, for the m th hidden layer with $m = 1, \dots, M$, we consider $d_k^{(m)}$ heterogeneous neurons specific to the k th subgroup and $d_0^{(m)}$ homogeneous neurons shared by all K subgroups, and $T_k^{(m)}(\mathbf{u}) = \mathbf{\Delta}_k^{(m)} \mathbf{u} + \mathbf{b}_k^{(m)}$ and $T_0^{(m)}(\mathbf{u}) = \mathbf{\Delta}_0^{(m)} \mathbf{u} + \mathbf{b}_0^{(m)}$ are affine transformations involving unknown parameters $\mathbf{\Delta}_k^{(m)} \in \mathbb{R}^{d_k^{(m)} \times d_k^{(m-1)}}$ and $\mathbf{b}_k^{(m)} \in \mathbb{R}^{d_k^{(m)} \times 1}$ and $\mathbf{\Delta}_0^{(m)} \in \mathbb{R}^{d_0^{(m)} \times d_0^{(m-1)}}$ and $\mathbf{b}_0^{(m)} \in \mathbb{R}^{d_0^{(m)} \times 1}$, respectively. $h(\cdot)$ is the activation function, which can be rectified linear unit (ReLU), sigmoid, tanh, and some others. In addition, an output layer with $T_k^{(M+1)}(\mathbf{u}) = \mathbf{\Delta}_k^{(M+1)} \mathbf{u} + \mathbf{b}_k^{(M+1)}$ is introduced for the output x_{ij} , with $\mathbf{\Delta}_k^{(M+1)} \in \mathbb{R}^{1 \times (d_k^{(M)} + d_0^{(M)})}$ and $\mathbf{b}_k^{(M+1)} \in \mathbb{R}^{1 \times 1}$, which integrates both the heterogeneous and homogeneous neurons. Denote

\mathbf{U}_k as a vector consisting of all parameters in the M hidden layers and output layer.

Based on (1) and (2), we further propose conducting joint network estimation for K cell subgroups and introduce the following penalized loss function in JRDNN:

$$l_{pn}(\mathbf{X}; \Phi) = \sum_{j=1}^p \left\{ - \sum_{i=1}^n \sum_{k=1}^K \tau_{ik} l_n(\mathbf{x}_i; \mathbf{U}_{kj}, \mathbf{w}_{k,j}, \pi_j) + \lambda_1 \sum_{l \neq j} \sum_{k=1}^K |w_{k,jl}| \right. \\ \left. + \lambda_2 \sum_{l \neq j} \sum_{k=1}^K \sum_{k' \neq k} |1(w_{k,jl} \neq 0) - 1(w_{k',jl} \neq 0)| + \lambda_3 \sum_{k=1}^K \|\Delta_k^{(1)}\|_F \right\}, \quad (3)$$

with $l_n(\mathbf{x}_i; \mathbf{U}_{kj}, \mathbf{w}_{k,j}, \pi_j) = \delta_{ij} \left[\log \pi_j - \frac{1}{2} \left\{ \log(2\pi_j) + (x_{ij} - g(\mathbf{x}_{i \setminus j}; \mathbf{U}_{kj}, \mathbf{w}_{k,j}))^2 \right\} \right] + (1 - \delta_{ij}) \log(1 - \pi_j)$, where \mathbf{X} is a $n \times p$ matrix consisting of $\mathbf{x}_1, \dots, \mathbf{x}_n$, Φ denotes all unknown parameters, $1(\cdot)$ is an indicator function, $\tau_{ik} = 1(C_i = k)$, $\delta_{ij} = 1(x_{ij} \neq 0)$, and λ_1, λ_2 , and λ_3 are three non-negative tuning parameters.

In (3), the first term is the negative log-likelihood function, which models the fit of our data. The second term, an ℓ_1 penalty, encourages sparsity in the selection layer parameters $w_{k,jl}$'s to facilitate sparse network estimation. The third and fourth terms are designed to accommodate the commonality among different cell subgroups. Specifically, for any pairs of j and l , the third term promotes $1(w_{k,jl} \neq 0) = 1(w_{k',jl} \neq 0)$, resulting in that $w_{k,jl}$ and $w_{k',jl}$ tend to be zero or nonzero simultaneously. Thus, the K subgroups potentially share some common edges. We further introduce the fourth term to accommodate the similarity in connection strength of the edges. Specifically, the fourth term imposes the F-norm on the weights $\Delta_k^{(1)}$ of heterogeneous neurons in the first layer, promoting the elements of $\Delta_k^{(1)}$ shrunk towards zero simultaneously and thus pruning all heterogeneous neurons in the M hidden layers. With (3), the constructed networks of different cell subgroups not only reflect heterogeneity but also exhibit common connections with similar strength.

2.2 Heterogeneous Analysis

In practice, the subgroup assignments C_i 's are not always observed. To accommodate the unknown cell heterogeneity, we propose adopting the K-means clustering with the Mahalanobis distance, which is defined as $dis_{ik} = \sqrt{(\mathbf{x}_i - \mathbf{o}_k)^T \boldsymbol{\Sigma}_k^{-1} (\mathbf{x}_i - \mathbf{o}_k)}$, where \mathbf{o}_k is the centroid of the k th subgroup and $\boldsymbol{\Sigma}_k$ is the covariance matrix for the p genes. Instead of estimating $\boldsymbol{\Sigma}_k$, we consider estimating the precision matrix $\boldsymbol{\Theta}_k = \boldsymbol{\Sigma}_k^{-1}$ (which describes the conditional dependence between any two genes given the rest) directly with the network constructed using JRDNN. Specifically, $\hat{\boldsymbol{\Theta}}_k = (\hat{\Theta}_{k,jl})_{p \times p}$ is estimated with $\hat{\Theta}_{k,jl} = \hat{\Theta}_{k,lj} = 1$ if $(j, l) \in \hat{E}_k$ and $\hat{\Theta}_{k,jl} = \hat{\Theta}_{k,lj} = 0$ otherwise, for $j \neq l$, and $\hat{\Theta}_{k,ll} = 1$, where $\hat{E}_k = \{(j, l) : \hat{w}_{k,jl} \neq 0 \text{ or } \hat{w}_{k,lj} \neq 0\}$ with $\hat{w}_{k,jl}$ being estimated using JRDNN. The proposed K-means clustering strategy effectively incorporates the network dependence among genes and takes into account heterogeneity attributed to both differential genes and gene relationships, leading to more accurate cell subgroup identification.

2.3 Computation

To obtain the final network estimation and cell subgroup identification results, we develop an iteration strategy (see Supplementary Algorithm S1) that conducts JRDNN and K-means clustering iteratively until convergence, where the subgroup memberships C_i 's obtained by the K-means clustering are delivered to JRDNN for joint estimation of multiple networks for the K cell subgroups and the estimated networks \hat{E}_k are used for computing the Mahalanobis distance in the K-means clustering. Specifically, for realizing the JRDNN step, we adopt the stochastic gradient descent (SGD) algorithm (see Supplementary Algorithm S2), which is implemented through the deep learning framework *Pytorch* in Python. To accommodate the discontinuity of the indicator function in (3), we adopt $1 - e^{-\frac{w_{k,jl}^2}{\xi}}$ to

approximate $1(w_{k,jl} \neq 0)$, where ξ is a small positive constant and controls the goodness and smoothness of approximation. For realizing the K-means clustering step, we develop an iteration algorithm (see Supplementary Algorithm S3) that iteratively conducts a search for the cluster centroids and assigns the cluster memberships based on the Mahalanobis distance.

There are multiple tuning parameters in the proposed algorithm. For determining the number of subgroups K , we employ the silhouette coefficient (Shahapure & Nicholas 2020), which maximizes the mean intra-cluster distance and minimizes the mean nearest-cluster distance simultaneously. For the three parameters in (3), instead of conducting the popular cross-validation, which is often time-consuming, we choose to consider some fixed values with the dependence on the numbers of subgroups and genes. Specifically, we set $\lambda_1 = \frac{1}{p}$, $\lambda_2 = \frac{1}{K\sqrt{p}}$, and $\lambda_3 = \frac{1}{K\sqrt{d^{(1)}}}$, where $d^{(1)} = d_0^{(1)} + \sum_{k=1}^K d_k^{(1)}$ is the width of the first layer of JRDNN. For the hyperparameters of DNN, we choose a learning rate of 0.001, batch size of 50, activation function *tanh*, 200 epochs, and three hidden layers.

3 Simulation

3.1 Simulation Settings

In simulation, we consider 3,000 ($n = 3,000$) cells from three subgroups ($K = 3$), with measurements for 100 genes ($p = 100$). For the subgroup sizes, two settings are considered, where the balanced design has 1,000 cells in each subgroup and the imbalanced design has 1,500, 900, and 600 cells in the three subgroups, respectively. For each subgroup, we consider the block-wise networks with ten unconnected sub-networks, which mimic the module-based properties of the practical biological networks. For each sub-network, two

types of network structure are examined. The first is a star-chain structure, where the sub-network has one of the following patterns: (1) star pattern, there is one central node connected with all other nodes, and the non-central nodes are not connected with each other; (2) chain pattern, only the adjacent nodes are connected. The second is a scale-free structure, where the degree distribution follows a power law distribution with the maximum degree being four. The toy examples of these two types of network structures are provided in Supplementary Figure S1. The ratio of the common edges shared by three subgroups is 30% for both types of network.

Based on the network, we consider the following mechanisms for generating the measurements x_{ij} 's. First, set a "core gene" j_1 in each sub-network, which is the central gene for the star pattern, the first gene for the chain pattern (denote the adjacent genes as j_1, j_2, \dots, j_{10}), and the hub gene with the largest degree for the scale-free pattern. Second, we simulate x_{ij_1} of the "core gene" j_1 from $N(0, 1)$, $N(5, 1)$, and $N(10, 1)$ for the three subgroups, respectively. Then, for the star pattern, we simulate $x_{ij_l} = f(x_{ij_1}) + \epsilon_i$ for the other nine non-central genes, and for the chain pattern, we simulate $x_{ij_{l+1}} = f(x_{ij_l}) + \epsilon_i$ for $l = 1, \dots, 9$ sequentially, where $f(\cdot)$ is a nonlinear function and $\epsilon_i \sim N(0, 1)$ is a random noise. Three settings with from simple to complex nonlinear relationships for $f(\cdot)$ are investigated, including $f(x) = \sqrt[3]{x}$ (simple), $f(x) = 0.25 \exp(x) + \sqrt[3]{x}$ (medium), and $f(x) = 3 \sin(x) + 0.25 \exp(x) + \sqrt[3]{x}$ (complex). For the scale-free pattern, we first sort the genes j_1, \dots, j_{10} by degree from largest to smallest and denoted N_{j_l} as the node sets that have edges with j_l , then simulate $x_{ij_l} = \sum_{j_k \in N_{j_l} \text{ and } k < l} f_k(x_{ij_k})$ for $l = 2, \dots, 10$ sequentially. Three settings for $f_k(\cdot)$'s are also considered, where all settings include polynomial term x^3 and interaction term $0.5x_1x_2$, and two additional terms \sqrt{x} and $(x_1 + x_2)^2$ (simple), $0.2 \exp(x)$ and $\log(x^2)$ (medium), and $0.2 \exp(x)$ and $\sin(x)$ (complex). We further simulate

three dropout levels, where [10%, 30%] (low), [20%, 40%] (medium), and [30%, 50%] (high) elements of x_{ij} 's are replaced by zero. As a result, there are a total of 36 scenarios, covering a wide spectrum with various types of network structures, various levels of nonlinear relationships and dropouts, and both balanced and imbalanced sample distributions.

3.2 Competing Methods

In addition to the proposed JRDNN-KM, we consider ten competing methods, including BLGGM, JGNsc, JSEM, SpQN, Normalizr, GENIE3, locCSN, CS-CORE, SC3, and Seurat. Among them, BLGGM (Wu & Luo 2022) is a Bayesian heterogeneous network analysis approach based on the zero-inflated Gaussian distribution, which can achieve multiple network estimation and subgroup identification simultaneously. Both JGNsc and JSEM conduct a heterogeneous network analysis with prior known subgroup information, where the common structures of networks among different cell subgroups are accommodated. Specifically, JGNsc (Dong et al. 2023) is a two-stage approach that first develops a Bayesian hybrid imputation method for accommodating zero-inflated data and then conducts joint graphical lasso for multiple network estimation. JSEM (Ma & Michailidis 2016) conducts a joint analysis of multiple networks using node-wise linear regressions incorporating a group lasso penalty. SpQN, Normalizr, GENIE3, LocCSN, and CS-CORE were all originally developed for a single network analysis. Specifically, SpQN (Wang et al. 2022) is a two-stage approach that first conducts normalizing local distributions in correlation matrices to remove the mean-correlation relationship and then adopts the graphical lasso to refine network estimation. Normalizr (Wang 2021) develops a normalization and statistical association testing framework to detect linear relationships with effective accommodation of the nonlinear confounders arising from library size. GENIE3 (Huynh-

Thu et al. 2010) explores the conditional dependence based on the node-wise nonlinear regression and adopts an ensemble of tree-based machine learning algorithms. LocCSN (Wang et al. 2021) proposes a nonparametric investigation of the joint distribution of gene expression and can detect nonlinear correlations. CS-CORE (Su et al. 2023) is an unconditional correlation-based distribution-free approach capable of addressing the high sequencing depth variations and measurement errors in scRNA-seq data. For these approaches based on the prior known subgroup information, we consider the true cell subgroup memberships and conduct JGNsc and JSEM for joint network analysis and conduct SpQN, Normalizr, GENIE3, LocCSN, and CS-CORE separately for each subgroup. SC3 (Kiselev et al. 2017) and Seurat (Butler et al. 2018) are two popular heterogeneous analysis methods for single-cell transcriptomic data, without accounting for network estimation, where SC3 is a consensus clustering method and Seurat is a graph-based clustering based on the projected space from PCA. BLGGM, JGNsc, JSEM, and CS-CORE are realized using R codes from <https://github.com/WgitU/BLGGM>, <https://github.com/meichendong/JGNsc>, <https://github.com/drjingma/JSEM>, and <https://github.com/ChangSuBiostats/CS-CORE>, respectively. Normalizr is realized using Python codes from <https://github.com/lingfeiwang/normalizr>. In addition, SpQN, GENIE3, SC3, and Seurat are realized using R packages *SpQN*, *GENIE3*, *SC3*, *Seurat*, respectively, and locCSN is realized using Python package *locCSN*.

3.3 Examination of the number of subgroups

Given the candidate values $\{1, 2, 3, 4, 5\}$ of K , we take the simulation scenarios under the balanced design and low dropout rate as examples and examine the performance of the silhouette coefficient for selecting K , where two types of network structure and three levels

of nonlinear relationships are considered. Specifically, the frequency at which a particular value is selected over 100 replicates is reported in Supplementary Table S1. In general, the silhouette coefficient consistently shows accurate identification of the true number of subgroups ($K = 3$). As expected, the more complex network structure (scale-free) and nonlinear relationships make it slightly more difficult to identify the true value of K .

3.4 Evaluation of heterogeneity analysis and network estimation

In the downstream analysis, we set $K = 3$ for all the methods to facilitate a more direct comparison and simulated 100 replicates under each scenario. The adjusted rand index (ARI) is adopted to assess the heterogeneity analysis performance, with values ranging from 0 to 1 and a larger value indicating a higher subgroup identification accuracy. In addition, we also employ Recall, Precision, and F1 score to evaluate the performance of network estimation, where the true and estimated edges are examined. Summarized ARI values and F1 scores over 100 replicates are provided in Figures 2 and 3, and the rest of the results are presented in Supplementary Figures S2 and S3. Here, ARI values for JGNsc, JSEM, SpQN, Normalizr, GENIE3, locCSN, and CS-CORE are not available since they are developed for network estimation and cannot identify unknown cell subgroups. In our study, we utilize true subgroup memberships for these methods. In addition, Recall, Precision, and F1 score are not available for SC3 and Seurat, as they do not conduct network estimation.

In Figure 2, JRDNN-KM demonstrate superior subgroup identification performance across all scenarios, especially as the level of sparsity intensifies and the complexity of nonlinear relationships increases. The benefits of JRDNN-KM that can effectively accommodate the nonlinear relationships among genes become increasingly apparent under these

challenging conditions. Under scenarios with imbalanced samples, the subgroup identification accuracy of all methods diminishes, potentially due to the reduced sample size within some subgroups. However, JRDNN-KM still achieves higher ARI values. In general, BLGMM performs the second best, as it accommodates both the network structure and high sparsity of data. With the focus on the differential expressions only, SC3 and Seurat have the lowest ARI values.

In addition to the satisfactory subgroup identification performance, in Figure 3, JRDNN-KM consistently outperforms the alternative methods in network estimation accuracy, with larger values of F1 across all scenarios. Notably, as shown in Supplementary Figure S2, when the degree of nonlinearity increases, the Recall values of all methods become smaller, particularly for those reliant on linear assumptions, such as BLGGM, JGNsc, SpQN, and Normaliser. The proposed JRDNN-KM, which is based on deep neural networks, displays marked advantages as the nonlinear complexity escalates. Additionally, with an increase in zero inflation, all methods experience a decline in the F1 value. However, JRDNN-KM can maintain its superiority even amid increased dropout occurrences. It also shows robustness in situations with imbalanced sample sizes, with no significant performance differences observed compared to balanced settings. With the ability to accommodate nonlinear relationships, GENIE3 and locCSN maintain better performance than methods based on linearity assumptions. CS-CORE, being a distribution-free method that does not rely on distributional assumptions and may have the potential to handle nonlinearities, achieves good performance in nonlinear situations as well. The superiority of JRDNN-KM over these three methods directly supports the proposed DNN strategy for more effectively addressing complex nonlinear relationships and simultaneously taking into account the commonality among different subgroups. Although with the true subgroup memberships, the GMM-

based JGNsc, JSEM, and SpQN lose effectiveness in the face of the complicated network structure, where JGNsc generally outperforms JSEM and SpQN by incorporating dropout. Overall, JRDNN-KM can achieve superior performance in both heterogeneity and network analysis, suggesting its practical usefulness in single-cell transcriptomic data analysis.

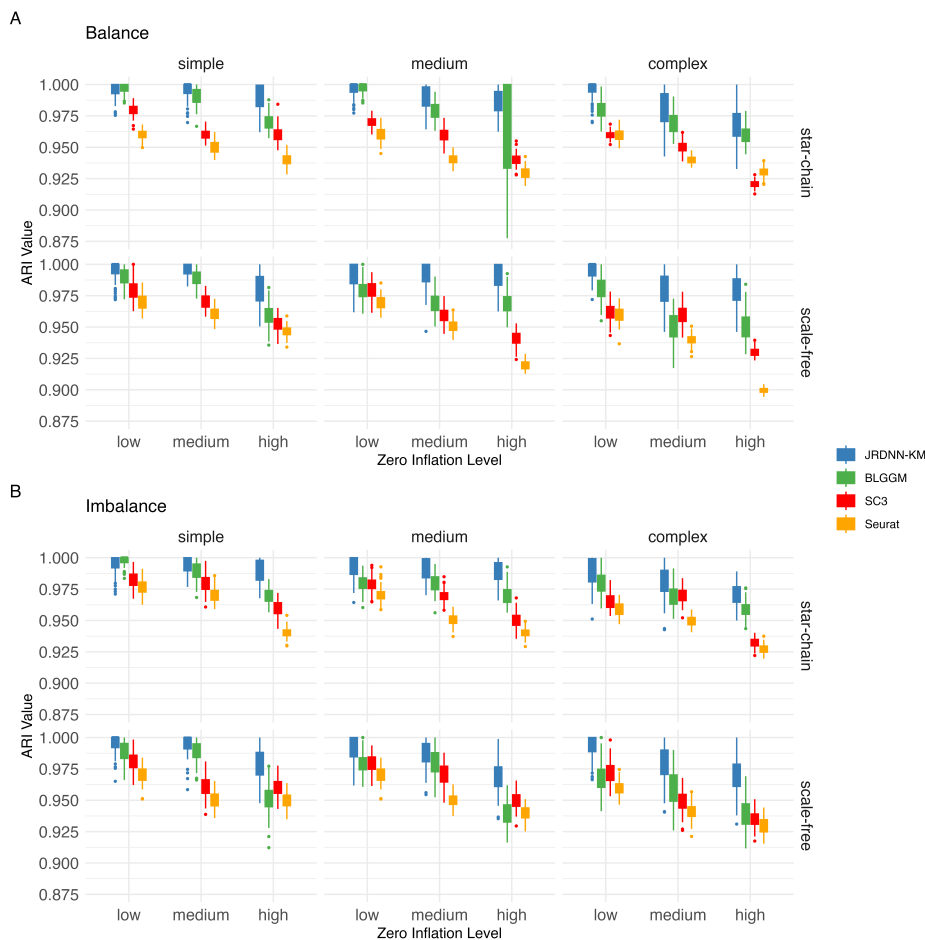


Figure 2: Summarized simulation results over 100 replicates with different methods. (A) and (B) Boxplots of ARI values under a balanced and imbalanced sample distribution, respectively. In each subfigure, two network structures (star-chain and scale-free), three levels of zero-inflation rate (low, medium, and high), and three levels of nonlinear relationships (simple, medium, and complex) are considered.

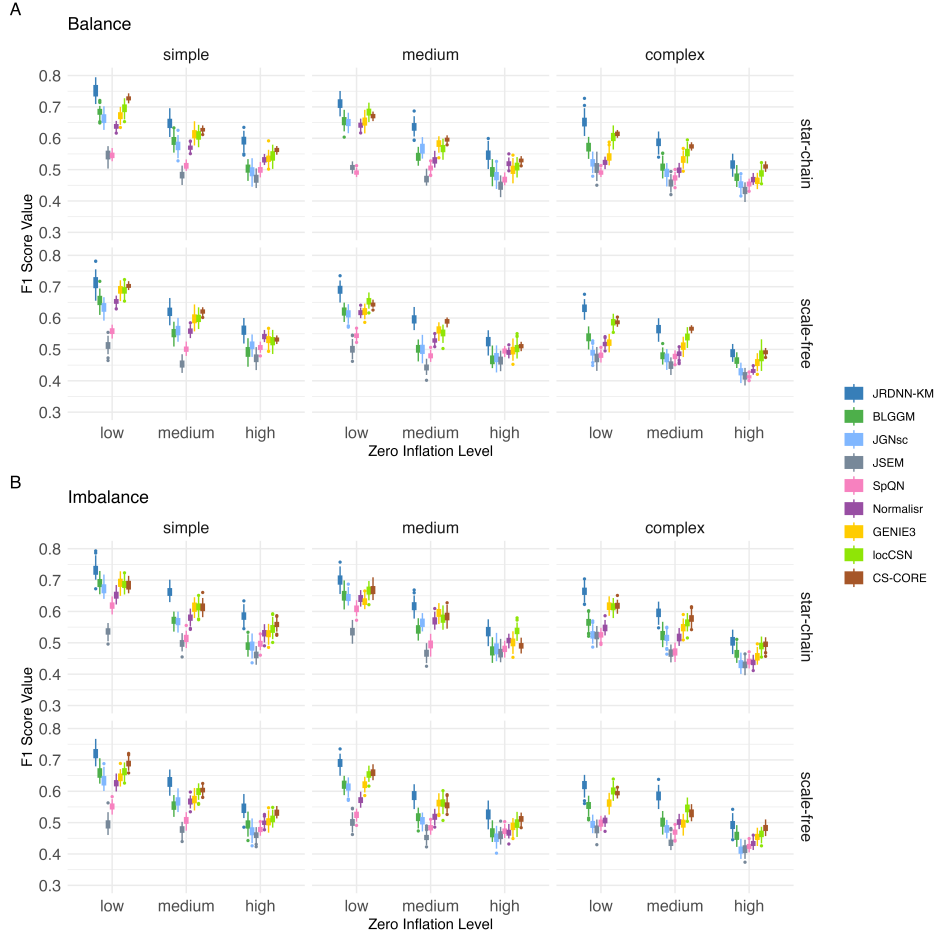


Figure 3: Summarized simulation results over 100 replicates with different methods. (A) and (B) of F1 scores under a balanced and imbalanced sample distribution, respectively. In each subfigure, two network structures (star-chain and scale-free), three levels of zero-inflation rate (low, medium, and high), and three levels of nonlinear relationships (simple, medium, and complex) are considered.

3.5 Sensitivity Analysis

We continue to investigate scenarios where only linear relationships exist among genes, leading to potential model misspecification for JRDNN-KM. Specifically, we consider the star-chain network structure with $f(x) = \beta x$, where $\beta \sim N(3, 1)$. Under the balanced design, various numbers of cells ($n = 3,000, 6,000, \text{ and } 9,000$) and dropout levels are ex-

amined. The corresponding summary results are reported in Supplementary Figure S4. Under these relatively simpler scenarios, the four heterogeneity analysis methods all have satisfactory subgroup identification accuracy, especially for JRDNN-KM and BLGGM, which achieve average ARI values of 1. In terms of network estimation accuracy, with the limited sample size ($n = 3000$), performance of JRDNN-KM is slightly weaker compared to strictly linear methods, such as BLGGM and JGNsc, due to the nonlinearity introduced by activation functions in DNN that may disrupt the inherent linearity. However, JRDNN-KM still outperforms the other nonlinear methods, GENIE3, locCSN, and CS-CORE, and the linear JSEM, SpQN, and Normalizr methods. When the sample size increases, JRDNN-KM demonstrates substantial improvements and even surpassed BLGGM and JGNsc, suggesting its effectiveness under the model misspecification.

Additionally, in Supplementary Table S2, we perform simulations with various levels of common information across different subgroups. Specifically, the balanced design with star-chain network, medium dropout rate, and medium nonlinear relationships are considered. It can be seen that for JRDNN-KM and JGNsc, which pay particular attention to the similarity among different subgroups, the increasing common information potentially facilitates a more accurate network estimation with a large value of F1. To further get deeper insights into the characteristics of JRDNN-KM, we also conduct ablation experiments. Specifically, under the scenarios with the balanced design, star-chain network, low dropout rate, and three levels of nonlinear relationships, we consider the proposed framework without the similarity regularization term or (and) the homogeneous hidden layers. Summary results are provided in Supplementary Table S3. It is observed that the proposed two techniques significantly contribute to both the heterogeneity analysis and network estimation. The significance is even more prominent under the scenarios with more complex

nonlinear relationships.

4 Application

We analyze five publicly available single-cell transcriptomic datasets, on human lung adenocarcinoma (LUAD) cell lines (Tian et al. 2019), human peripheral blood mononuclear cells (PBMC) (Zheng et al. 2017), mouse embryonic stem cells (mESCs) (Kolodziejczyk et al. 2015), and mouse liver and uterus cells from the Mouse Cell Atlas (MCA) (Han et al. 2018). In each of these five datasets, every cell has been carefully labeled with cell or lineage markers. These labels have been served as gold standards, enabling objective evaluation of the cell subgroup identification performance. To control the quality of datasets, we follow the published studies and remove cells expressing less than 500 genes and genes expressed in less than 100 cells. Summary information of these five datasets is provided in Table 1, including the numbers of cells and genes, proportion of zeros, and subgroup information. These five datasets vary in sample size from small (mESCs) to large (PBMC) and are in data quality from high with a low zero-inflation rate (mESCs) to poor with zero-inflation rates exceeding 90% (PBMC). The sample distributions across different subgroups also show diversity, where the mouse uterus data has a highly imbalanced sample distribution.

All data are then subjected to batch effect correction using MNN (Haghverdi et al. 2018), normalized for library size using the total count normalization (TC) method (Cole et al. 2019), and filtered for 100 highly variable genes using the variance stabilizing transformation (vst) method in R package “Seruat” (Hafemeister & Satija 2019).

Table 1: Summary information of the five real datasets

Dataset	No. of cells	No. of genes	Proportion of zeros	Subgroup information
LUAD	1,401	12,997	41.16%	H2228 (461), H1975 (519), HCC827 (421)
PBMC	12,418	8,560	91.12%	CD19+B (2,341), CD4+/CD25 Reg T (4,683), CD56+NK (5,394)
mESCs	704	15,618	30.77%	2i (295), a2i (159), lif (250)
Mouse Liver	2,116	6,673	90.13%	Dentritic (336), Endothelial (621), Erythroblast (199), Kupffer (768), T (192)
Mouse Uterus	2,313	6,237	86.39%	Endothelial (124), Glandular (232), Macrophage (141), Muscle (223), NK (135), Stromal (1,458)

4.1 JRDNN-KM leads to biologically sensible cell subgroups

We first consider the candidate sequence $\{2, 3, \dots, 8, 9, 10\}$ for K . For JRDNN-KM, the silhouette coefficient identifies three subgroups for all the LUAD, PBMC, and mESCs datasets, and five and six subgroups for the mouse liver and uterus datasets, respectively. The true numbers of cell subgroups are all identified correctly. For making a fair comparison, in the following analysis, K is set as the true number of cell subgroups for all methods, which has been usually considered in recent single-cell transcriptomic data analysis (Li et al. 2023).

The ARI values with JRDNN-KM as well as three competing methods are provided in Figure 4(A). The proportions of identified cell subgroups with JRDNN-KM in the true cell subgroups are reported in Figure 4(B) and the results with alternatives are reported in Supplementary Figure S5. It is observed that JRDNN-KM has superior or competitive per-

formance across multiple datasets with satisfactory ARI values. Specifically, in the LUAD dataset, JRDNN-KM achieves an ARI value of 1.00. This performance markedly outstrips other alternative methods. Additionally, JRDNN-KM maintains higher performance metrics across diverse cellular contexts, including PBMC, mESCs, and mouse uterus cells, where the mouse uterus dataset has a highly imbalanced sample distribution with some subgroups having a small number of cells. For the mouse liver cell data, which has a high dropout rate (90.13%) and small sample size, JRDNN-KM performs slightly worse than BLGMM, probably due to the fact that the DNN strategy usually demands a relatively large sample size, but still behaves much better than SC3 and Seurat. Although there is a certain degree of mis-identification for some datasets, Figure 4(B) shows that each true subgroup is dominated by one of the subgroups identified with JRDNN-KM, further validating its utility in precision oncology and regenerative medicine. Similar to simulation, the two methods, SC3 and Seurat, that do not accommodate the network structure among genes, always have inferior cell subgroup identification accuracy.

4.2 JRDNN-KM constructs heterogeneous networks with common edges

The inferred networks with JRDNN-KM are shown in Figure 5 for the LUAD dataset and Supplementary Figures S6-S9 for the rest four datasets. The identified numbers of edges for different subgroups are reported in Supplementary Figure S10-S14, where 70, 88, 76, 2, and 0 common edges are shared by all subgroups for the LUAD, PBMC, mESCs, and mouse liver and uterus datasets, respectively. The numbers of common edges for the mouse liver and uterus datasets are smaller compared to the other three datasets. This is reasonable, as the corresponding cell subgroups have relatively larger diversities. We

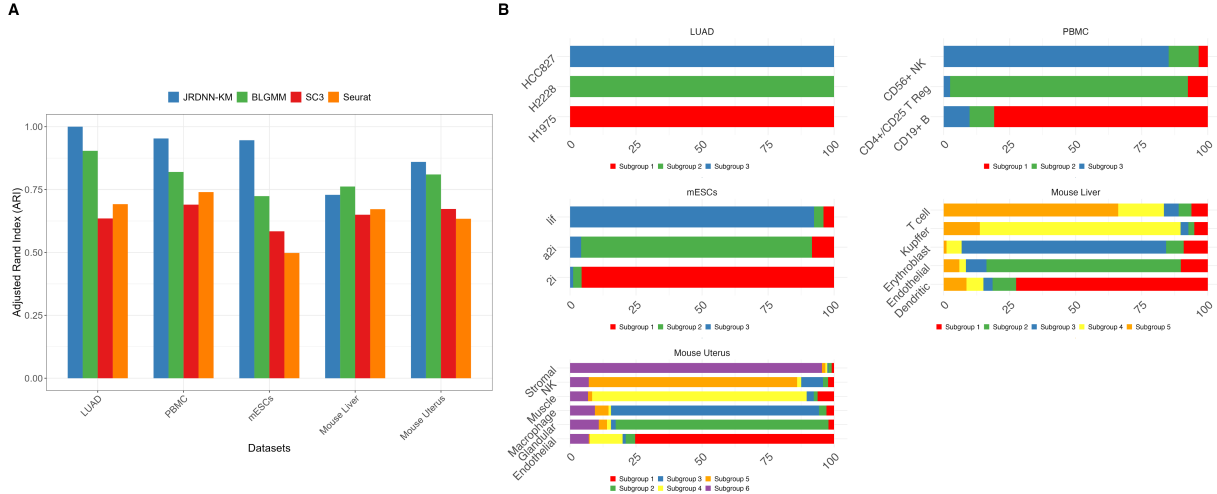


Figure 4: Heterogeneity analysis results on five real single-cell transcriptomic datasets. (A) ARI values with different methods. (B) Proportions of identified cell subgroups with JRDNN-KM in the true cell subgroups.

take a closer look at the Kupffer and T cell subgroups for the mouse liver dataset, which both participate in the regulation process of the immune system, and identify 71 common edges. For the mouse uterus dataset, we also examine the two immune regulation-related cell subgroups, Macrophage and NK cells, and identifies 26 common edges. In addition, 28 common edges are shared by the Endothelial and Muscle cells, which both participate in maintaining the normal physiological functions of the body. We also conduct analysis with the alternative methods, where the true cell subgroup memberships are adopted for JGNsc, JSEM, SpQN, Normalizr, GENIE3, locCSN, and CS-CORE, and present the comparison results in Supplementary Figure S10-S14. It can be seen that the nine methods identify a moderate number of overlapping edges, where the overlapping ratio of the identified edges between the proposed method and others lies in $[52.7\%, 82.8\%]$, and JRDNN-KM can effectively exploit the common information across different subgroups.

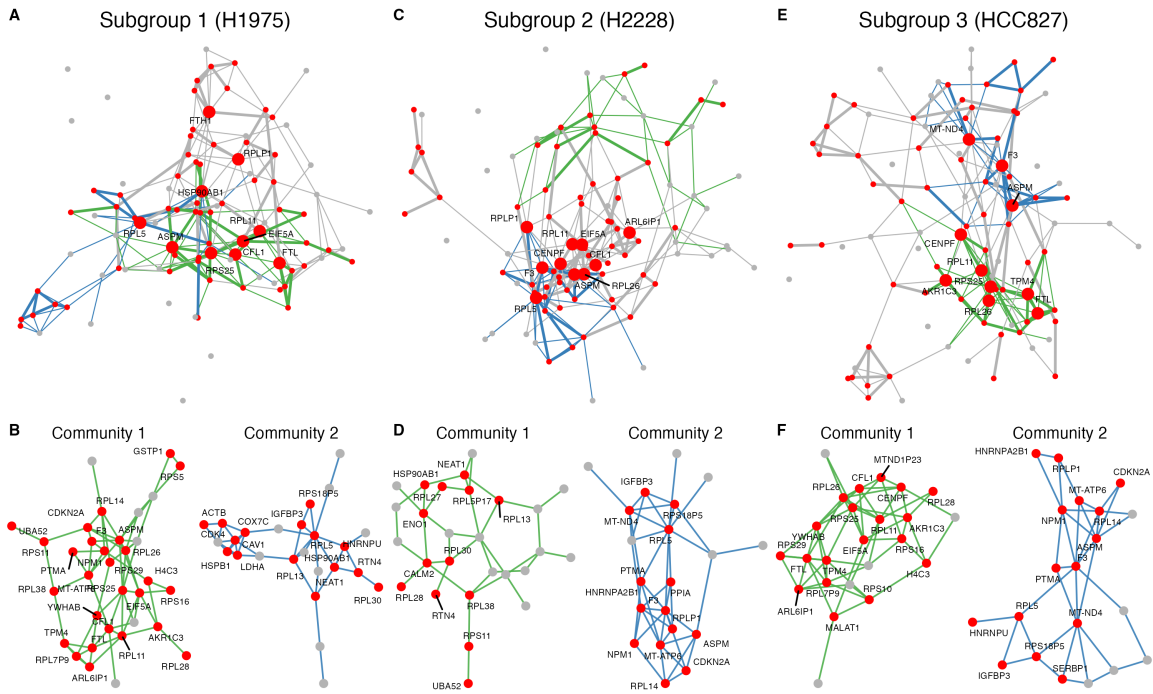


Figure 5: Networks constructed with JRDNN-KM for subgroup 1 (A), subgroup 2 (C), and subgroup 3 (E) of the LUAD dataset, where the common connections across all subgroups are highlighted by thick edges with involved genes highlighted with red color, and the hub genes with the top ten largest degrees are highlighted with a bigger point. (B), (D), and (F): Two representative communities detected using the Louvain algorithm for subgroup 1, subgroup 2, and subgroup 3, respectively.

4.3 Investigation of hub genes for the LUAD data

We further take the LUAD data from humans as an example and investigate the hub genes in the inferred networks with JRDNN-KM. The hub genes are important topological features of networks that usually have functional relevance. In this study, we consider the top ten genes with the largest degrees in the networks (shown in Supplementary Table S4 and highlighted with a bigger point in Figure 5 and Supplementary Figures S6-S9). It can be seen that JRDNN-KM identifies two common hub genes (RPR11 and ASPM) shared by all three cell lines (H1975, H2228, and HCC827) and nine common hub genes shared by

two of the three cell lines. The similarity across these three cell lines has been universally recognized in the literature. In addition, two specific hub genes (FTH1 and HSP90AB1), one specific gene (ARL6IP1), and three specific genes (MT-ND4, AKR1C3, and TPM4) are identified for subgroup 1 (H1975), subgroup 2 (H2228), and subgroup 3 (HCC827), respectively.

The top ten hub genes identified with the alternatives and the comparison results among different methods are also reported in Supplementary Table S4. It is observed that JRDNN-KM detects a few well-known marker genes that are found by the majority of approaches and also reveals some promising novel findings. Specifically, the two common hub genes, RPL11 and ASPM, shared by all three cell lines, are also recognized by most of the competing methods. Here, ASPM has emerged as a critical player in cancer biology, specifically influencing cancer aggressiveness and stemness. ASPM’s overexpression in various malignancies has been demonstrated to be strongly associated with poor patient outcomes, underscoring its role in oncogenic processes and its impact on cancer cell behavior and tumor evolution (Tsai et al. 2023). In addition, RPL11 is crucial in cancer progression through its interaction with the MDM2-P53 pathway. In particular, RPL11 acts as a tumor suppressor by stabilizing P53, particularly when PICT1 is deficient with the inhibition of MDM2’s activity, which correlates with slower tumor growth and potentially improved patient outcomes (Sasaki et al. 2011).

We further examine the subgroup-specific hub genes, where JRDNN-KM demonstrates its unique capability by recognizing hub genes that most competing methods missed. For instance, in the H1975 cell line, the FTL gene and in the HCC827 cell line, the AKR1C3 gene are only identified by JRDNN-KM and locCSN. These methods, both employing non-linear approaches, effectively highlight the non-linear regulatory relationships among

certain genes in LUAD, which might be overlooked before. Additionally, the CFL1 gene in the H2228 cell line is recognized only by JRDNN-KM. Biological implications of these genes have been well recognized in the literature. Specifically, the FTL gene plays a pivotal role in regulating ferroptosis by controlling iron storage and reducing oxidative stress under the governance of the NRF2 pathway. This regulation helps LUAD cells evade ferroptosis, thereby contributing to potential treatment resistance (Ding et al. 2024). AKR1C3 is consistently overexpressed in tumor tissues, suggesting its significant association with the disease and indicating its involvement in tumor progression and resistance to erlotinib therapy in LUAD (Cho et al. 2024). In addition, the CFL1 gene and its functional gene network have been suggested as prognostic biomarkers for lung adenocarcinoma, which can also guide chemotherapeutic interventions (Castro et al. 2010).

4.4 Community detection and GO enrichment analysis for the LUAD data

We continue to conduct community (module) detection on the referred networks using the Louvain algorithm and show two communities with the largest sizes in Figure 5 and Supplementary Figures S6-S9. Both homogeneous and heterogeneous edges are observed in these communities. Similar to the analysis on the hub genes, a deeper examination based on the gene ontology (GO) enrichment analysis is conducted for the LUAD data, where the top five GO terms with the smallest P-values for each subgroup are presented in Figure 6. The results suggest that the communities share some significantly enriched GO terms, indicating functional and biological connections among the related genes. The community detection analysis is also conducted for the competing methods, and the top ten significant GO terms involved in the two largest communities are reported in Supplementary Tables

S5-S7. It can be seen that some GO terms are shared by all the nine methods. Compared to the H1975 and H2228 cell lines, JRDNN-KM has more unique findings in the HCC827 cell line.

Specifically, as shown in Figure 6, “cytoplasmic translation” is among the top five significant GO terms in all three subgroups. This biological process has been found to be crucial as it facilitates the synthesis of proteins necessary for cancer cell growth and proliferation and is notably involved in the progression of LUAD. In addition, the p53 class mediator-related GO terms are significantly enriched in both H2228 and HCC827 cell lines. Although not featured among the top five significant terms, these terms are also significant in the H1975 cell line, specifically the “regulation of signal transduction by p53 class mediator” with a p-value of 4.736×10^{-4} , and “positive regulation of signal transduction by p53 class mediator” with a p-value of 7.894×10^{-4} . In LUAD, p53 has been shown to suppress tumor development by promoting the differentiation of alveolar type 1 (AT1) cells from transitional states during alveolar repair, effectively governing cell state to prevent the persistence of cancerous cell types and maintain lung tissue integrity (Kaiser et al. 2023). These two terms are also detected by all competing methods with significant p-values.

Similar to the analysis of hub genes, JRDNN-KM identifies some unique GO terms, such as “regulation of translation” found only by JRDNN-KM and locCSN in the H1975 cell line and “regulation of protein modification” discovered only by JRDNN-KM in the HCC827 cell line, suggesting that JRDNN-KM reveals relevant novel biological processes. Recent research shows that in the H1975 cell line, significant alterations in translation regulators were observed, particularly in rociletinib-resistant cells. These changes may affect the synthesis of key proteins, potentially influencing tumor progression and response

to therapy (Zhang et al. 2021). And in HCC827 cells, inhibiting N-linked glycosylation, a key protein modification, disrupts EGFR function, reducing proliferation and inducing senescence (Lopez-Sambrooks et al. 2016). These unique findings of JRDNN-KM correlate well with practical biological explanations, providing valuable insights for research and clinical applications.

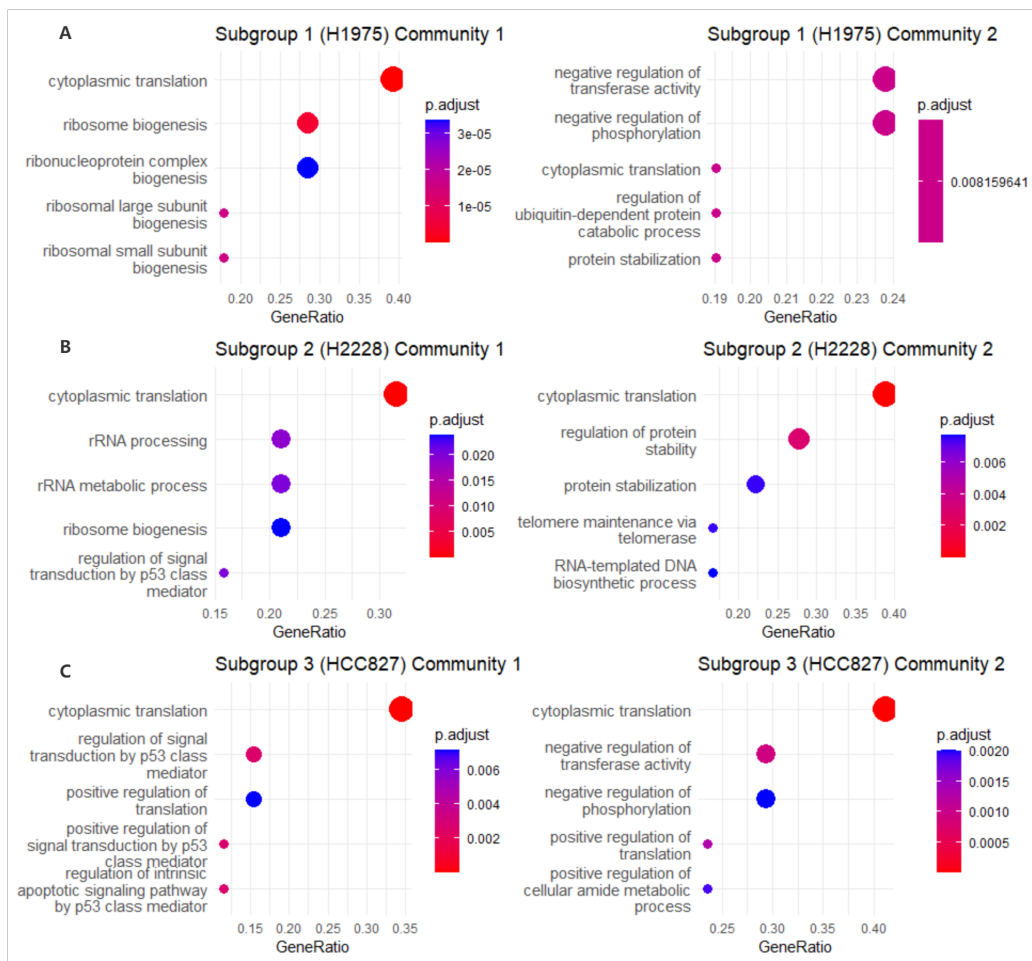


Figure 6: GO enrichment analysis results of two representative communities identified with JRDNN for the LUAD data. (A) Subgroup 1, (B) Subgroup 2, and (C) Subgroup 3.

5 Discussion

In this study, we have proposed JRDNN-KM, a systemic statistical framework for estimating heterogeneous networks and cell subgroups from single-cell transcriptomic data. JRDNN-KM has leveraged the robust fitting capabilities of neural networks to approximate the complex nonlinear relationships between genes and incorporated the inferred networks into the K-means clustering to accommodate both the mean and covariance heterogeneous among cell subgroups. JRDNN-KM has directly addressed the challenging characteristics of single-cell transcriptomic data, including the nonlinearity, zero-inflation, unknown cellular heterogeneity, as well as a certain degree of homogeneity among cell subgroups. Under extensive simulation studies, JRDNN-KM has demonstrated substantial improvements over recent network estimation models, particularly in handling complex nonlinear relationships among genes that are not adequately captured by models such as GGMs.

Our analyses of real single-cell transcriptomic data from various sources have further validated the utility of JRDNN-KM. Besides the accurate cell subgroup identification performance, the networks identified by JRDNN-KM have been consistently corroborated by biological research. On one hand, the biologically implicated common hub genes and significant GO terms shared by different cell subgroups highlight JRDNN-KM’s potential in investigating the homogeneous dependencies and interactions among genes in the same tissue. On the other hand, the heterogeneous topological properties of the inferred networks providing deeper insights into the subgroup specific-cellular mechanisms underlying different biological states and conditions. These two different types of characteristics are crucial for practical applications in biomedical research and therapy development.

Our study, while groundbreaking, acknowledges certain limitations. For instance, our proposed loss function is based on squared loss, which may lack robustness against outliers

and noise. Future work could explore optimizing this aspect to enhance the model’s stability and performance under varying conditions. Additionally, our assumptions regarding zero inflation are based on varying zero-inflation rates across different genes. However, emerging research indicates that technical dropout may be correlated with expression levels, suggesting a need for a more nuanced approach to account for these dependencies in our model. Due to computational constraints, our study necessitates preprocessing the data before applying our JRDNN-KM method. Future work will concentrate on refining the model to enhance its capacity to handle even larger datasets, thereby broadening its applicability across various areas of genomics.

Overall, JRDNN-KM represents a significant advancement in the field of single-cell genomics, offering a powerful tool for researchers exploring the intricate landscape of gene dependence and interactions at the single-cell level.

Funding

This research was supported by the National Natural Science Foundation of China (12071273); Shanghai Rising-Star Program (22QA1403500); Shanghai Science and Technology Development Funds (23JC1402100); Shanghai Research Center for Data Science and Decision Technology; National Institutes of Health (CA204120 and CA121974); and National Science Foundation (2209685).

Disclosure Statement

The authors report there are no competing interests to declare.

Supplementary Materials

Additional supporting information may be found online in the supplementary materials section at the end of the article.

Supplement.pdf Supplementary Materials for “Heterogeneous network estimation for single-cell transcriptomic data via a joint regularized deep neural network”, including the details of the proposed algorithms and additional settings and results of simulation studies and real data analysis.

JRDNN-KM.zip The package JRDNN-KM that implements the proposed approach, which is available at <https://github.com/mengyunwu2020/JRDNN-KM>.

References

- Booeshaghi, A. S. & Pachter, L. (2021), ‘Normalization of single-cell RNA-seq counts by $\log(x+1)$ or $\log(1+x)$ ’, *Bioinformatics* **37**(15), 2223–2224.
- Butler, A., Hoffman, P., Smibert, P., Papalexi, E. & Satija, R. (2018), ‘Integrating single-cell transcriptomic data across different conditions, technologies, and species’, *Nature Biotechnology* **36**(5), 411–420.
- Cai, T. T., Liu, W. & Zhou, H. H. (2016), ‘Estimating sparse precision matrix: Optimal rates of convergence and adaptive estimation’, *The Annals of Statistics* **44**, 455–488.
- Castro, M. A. A., Dal-Pizzol, F., Zdanov, S., Soares, M., Müller, C. B., Lopes, F. M., Zanotto-Filho, A., Fernandes, M. d. C., Moreira, J. C. F., Shacter, E. et al. (2010), ‘CFL1 expression levels as a prognostic and drug resistance marker in nonsmall cell lung cancer’, *Cancer* **116**(15), 3645–3655.

- Cho, W. C., Li, K. P., Wong, C. F., Fung, K. Y., Chow, J. C., Cheung, K. M., Chan, J. C. & Lau, E. Y. (2024), ‘Exploring AKR1C3 as a therapeutic target to overcome erlotinib resistance in lung adenocarcinoma’, *Cancer Research* **84**(6_Supplement), 5958–5958.
- Cole, M. B., Risso, D., Wagner, A., DeTomaso, D., Ngai, J., Purdom, E., Dudoit, S. & Yosef, N. (2019), ‘Performance assessment and selection of normalization procedures for single-cell RNA-seq’, *Cell Systems* **8**(4), 315–328.
- Costanzo, M., Kuzmin, E., van Leeuwen, J., Mair, B., Moffat, J., Boone, C. & Andrews, B. (2019), ‘Global genetic networks and the genotype-to-phenotype relationship’, *Cell* **177**(1), 85–100.
- Ding, Y., Gao, J., Chen, J., Ren, J., Jiang, J., Zhang, Z., Tong, X. & Zhao, J. (2024), ‘Bub1b impairs chemotherapy sensitivity via resistance to ferroptosis in lung adenocarcinoma’, *Cell Death & Disease* **15**(7), 525.
- Dong, M., He, Y., Jiang, Y. & Zou, F. (2023), ‘Joint gene network construction by single-cell RNA sequencing data’, *Biometrics* **79**(2), 915–925.
- Gawad, C., Koh, W. & Quake, S. R. (2016), ‘Single-cell genome sequencing: current state of the science’, *Nature Reviews Genetics* **17**(3), 175–188.
- Hafemeister, C. & Satija, R. (2019), ‘Normalization and variance stabilization of single-cell RNA-seq data using regularized negative binomial regression’, *Genome Biology* **20**(1), 296.
- Haghverdi, L., Lun, A. T., Morgan, M. D. & Marioni, J. C. (2018), ‘Batch effects in single-cell RNA-sequencing data are corrected by matching mutual nearest neighbors’, *Nature Biotechnology* **36**(5), 421–427.

- Halama, A., Zaghlool, S., Thareja, G., Kader, S., Al Muftah, W., Mook-Kanamori, M., Sarwath, H., Mohamoud, Y. A., Stephan, N., Ameling, S. et al. (2024), ‘A roadmap to the molecular human linking multiomics with population traits and diabetes subtypes’, *Nature Communications* **15**(1), 7111.
- Han, X., Wang, R., Zhou, Y., Fei, L., Sun, H., Lai, S., Saadatpour, A., Zhou, Z., Chen, H., Ye, F. et al. (2018), ‘Mapping the mouse cell atlas by microwell-seq’, *Cell* **172**(5), 1091–1107.
- Huynh-Thu, V. A., Irrthum, A., Wehenkel, L. & Geurts, P. (2010), ‘Inferring regulatory networks from expression data using tree-based methods’, *PLoS One* **5**(9), e12776.
- Kaiser, A. M., Gatto, A., Hanson, K. J., Zhao, R. L., Raj, N., Ozawa, M. G., Seoane, J. A., Biegging-Rolett, K. T., Wang, M., Li, I. et al. (2023), ‘p53 governs an at1 differentiation programme in lung cancer suppression’, *Nature* **619**(7971), 851–859.
- Karaaslanli, A., Saha, S., Maiti, T. & Aviyente, S. (2023), ‘Kernelized multiview signed graph learning for single-cell RNA sequencing data’, *BMC Bioinformatics* **24**(1), 127.
- Kiselev, V. Y., Kirschner, K., Schaub, M. T., Andrews, T., Yiu, A., Chandra, T., Natarajan, K. N., Reik, W., Barahona, M., Green, A. R. et al. (2017), ‘SC3: consensus clustering of single-cell RNA-seq data’, *Nature Methods* **14**(5), 483–486.
- Kolodziejczyk, A. A., Kim, J. K., Tsang, J. C., Ilicic, T., Henriksson, J., Natarajan, K. N., Tuck, A. C., Gao, X., Bühler, M., Liu, P. et al. (2015), ‘Single cell RNA-sequencing of pluripotent states unlocks modular transcriptional variation’, *Cell Stem Cell* **17**(4), 471–485.
- Li, Y., Wu, M., Ma, S. & Wu, M. (2023), ‘Zinbmm: a general mixture model for simultane-

- ous clustering and gene selection using single-cell transcriptomic data’, *Genome Biology* **24**(1), 208.
- Lopez-Sambrooks, C., Shrimal, S., Khodier, C., Flaherty, D. P., Rinis, N., Charest, J. C., Gao, N., Zhao, P., Wells, L., Lewis, T. A. et al. (2016), ‘Oligosaccharyltransferase inhibition induces senescence in rtk-driven tumor cells’, *Nature Chemical Biology* **12**(12), 1023–1030.
- Ma, J. & Michailidis, G. (2016), ‘Joint structural estimation of multiple graphical models’, *The Journal of Machine Learning Research* **17**(1), 5777–5824.
- McDavid, A., Gottardo, R., Simon, N. & Drton, M. (2019), ‘Graphical models for zero-inflated single cell gene expression’, *The Annals of Applied Statistics* **13**(2), 848–873.
- Nguyen, T. K. H., Van den Berge, K., Chiogna, M. & Risso, D. (2023), ‘Structure learning for zero-inflated counts with an application to single-cell RNA sequencing data’, *The Annals of Applied Statistics* **17**(3), 2555–2573.
- Oh, J., Chang, C. & Long, Q. (2023), ‘Accounting for technical noise in Bayesian graphical models of single-cell RNA-sequencing data’, *Biostatistics* **24**(1), 161–176.
- Sasaki, M., Kawahara, K., Nishio, M., Mimori, K., Kogo, R., Hamada, K., Itoh, B., Wang, J., Komatsu, Y., Yang, Y. R. et al. (2011), ‘Regulation of the mdm2-p53 pathway and tumor growth by pict1 via nucleolar rpl11’, *Nature Medicine* **17**(8), 944–951.
- Shahapure, K. R. & Nicholas, C. (2020), Cluster quality analysis using silhouette score, in ‘2020 IEEE 7th International Conference on Data Science and Advanced Analytics (DSAA)’, IEEE, pp. 747–748.

- Su, C., Xu, Z., Shan, X., Cai, B., Zhao, H. & Zhang, J. (2023), ‘Cell-type-specific co-expression inference from single cell rna-sequencing data’, *Nature Communications* **14**(1), 4846.
- Tian, L., Dong, X., Freytag, S., Lê Cao, K.-A., Su, S., JalalAbadi, A., Amann-Zalcenstein, D., Weber, T. S., Seidi, A., Jabbari, J. S. et al. (2019), ‘Benchmarking single cell RNA-sequencing analysis pipelines using mixture control experiments’, *Nature Methods* **16**(6), 479–487.
- Tsai, K. K., Bae, B.-I., Hsu, C.-C., Cheng, L.-H. & Shaked, Y. (2023), ‘Oncogenic aspm is a regulatory hub of developmental and stemness signaling in cancers’, *Cancer Research* **83**(18), 2993–3000.
- Wang, H., Lengerich, B. J., Aragam, B. & Xing, E. P. (2019), ‘Precision lasso: accounting for correlations and linear dependencies in high-dimensional genomic data’, *Bioinformatics* **35**(7), 1181–1187.
- Wang, L. (2021), ‘Single-cell normalization and association testing unifying crispr screen and gene co-expression analyses with normalizr’, *Nature Communications* **12**(1), 6395.
- Wang, X., Choi, D. & Roeder, K. (2021), ‘Constructing local cell-specific networks from single-cell data’, *Proceedings of the National Academy of Sciences* **118**(51), e2113178118.
- Wang, Y., Hicks, S. C. & Hansen, K. D. (2022), ‘Addressing the mean-correlation relationship in co-expression analysis’, *PLoS Computational Biology* **18**(3), e1009954.
- Wu, N., Yin, F., Ou-Yang, L., Zhu, Z. & Xie, W. (2020), ‘Joint learning of multiple gene networks from single-cell gene expression data’, *Computational and Structural Biotechnology Journal* **18**, 2583–2595.

- Wu, Q. & Luo, X. (2022), ‘Estimating heterogeneous gene regulatory networks from zero-inflated single-cell expression data’, *The Annals of Applied Statistics* **16**(4), 2183–2200.
- Xiao, F., Tang, J., Fang, H. & Xi, R. (2022), ‘Estimating graphical models for count data with applications to single-cell gene network’, *Advances in Neural Information Processing Systems* **35**, 29038–29050.
- Zhang, T. & Zou, H. (2014), ‘Sparse precision matrix estimation via lasso penalized D-trace loss’, *Biometrika* **101**(1), 103–120.
- Zhang, X., Maity, T. K., Ross, K. E., Qi, Y., Cultraro, C. M., Bahta, M., Pitts, S., Keswani, M., Gao, S., Nguyen, K. D. P. et al. (2021), ‘Alterations in the global proteome and phosphoproteome in third generation egfr tki resistance reveal drug targets to circumvent resistance’, *Cancer Research* **81**(11), 3051–3066.
- Zheng, C. & Tang, E. (2024), ‘A topological mechanism for robust and efficient global oscillations in biological networks’, *Nature Communications* **15**(1), 6453.
- Zheng, G. X., Terry, J. M., Belgrader, P., Ryvkin, P., Bent, Z. W., Wilson, R., Ziraldo, S. B., Wheeler, T. D., McDermott, G. P., Zhu, J. et al. (2017), ‘Massively parallel digital transcriptional profiling of single cells’, *Nature Communications* **8**(1), 14049.